

Preprint 02-2007

Ruhr University Bochum
Lehrstuhl für Technische Mechanik

**A novel variational algorithmic formulation
for wrinkling at finite strains based on
energy minimization: application to mesh
adaption**

J. Mosler

This is a preprint of an article accepted by:
*Computer Methods in Applied Mechanics and
Engineering* (2007)

A novel variational algorithmic formulation for wrinkling at finite strains based on energy minimization: application to mesh adaption

J. Mosler

Lehrstuhl für Technische Mechanik
Ruhr University Bochum
Universitätsstr. 150, D-44780 Bochum, Germany
E-Mail: mosler@tm.bi.ruhr-uni-bochum.de
URL: www.tm.bi.ruhr-uni-bochum.de/mosler

SUMMARY

This paper is concerned with an efficient novel algorithmic formulation for wrinkling at finite strains. In contrast to previously published numerical implementations, the advocated method is fully variational. More precisely, the parameters describing wrinkles or slacks, together with the unknown deformation mapping, are computed jointly by minimizing the potential energy of the considered mechanical system. Furthermore, the wrinkling criteria are naturally included within the presented variational framework. The proposed method allows to employ three-dimensional constitutive models without any additional modification, i.e., a projection in plane stress space is not required. Analogously to the wrinkling parameters, the non-vanishing out-of-plane component of the strain tensor results conveniently from relaxing the respective Helmholtz energy of the membrane. The proposed framework is very general and does not rely on any assumption regarding the symmetry of the material, i.e., arbitrary anisotropic hyperelastic models can be consistently taken into account. The advantages associated with such a variational method are manifold. For instance, it opens up the possibility of applying standard optimization algorithms to the numerical implementation. This is especially important for highly non-linear or singular problems such as wrinkling. On the other hand, minimization principles provide a suitable basis for a posteriori error estimation and thus, for adaptive finite element formulations. As a prototype, a variational error indicator leading to an efficient h -adaption for wrinkling is briefly discussed. The performance of the wrinkling approach is demonstrated by selected finite element analyses.

1 Introduction

Many design concepts in practical engineering are based on membrane structures. Particularly, in applications where weight is an issue such as in aerospace industries, lightweight membranes are frequently employed. One state-of-the-art example is given by solar sails. Nowadays, much research is focused on those sails which seem to be a promising way for energy generation in space.

Although the aforementioned application is relatively new, mechanical models for membranes date back, at least, to the pioneering work by Wagner [1] and Reissner [2]. Since then, Reissner's so-called *tension field theory* has been adopted and further elaborated by several researchers, cf., e.g. [3–7]. For a detailed overview on this theory, the interested reader is referred to the comprehensive work by Steigmann [8] and references cited therein. All the quoted works

have in common that either by modifying the considered constitutive law or by enhancing the strain tensor, the stresses are altered such that compression is avoided (tension field theory). Clearly, the assumption of vanishing compressive stresses represents an idealization.

Alternatively, it is possible to approximate wrinkles occurring in membranes explicitly. For instance, in [9, 10] wrinkling is modeled by using a shell-type formulation and considering a very small bending stiffness (thin shell). One advantage of such a method is that the assumption known from tension field theory is not required. Furthermore, in some applications, the bending stiffness does play an important role. In such cases, it can be consistently taken into account by using (bending) shells. For example, in [11, 12] folding in thin-films was analyzed by applying a von Kármán plate theory. Within the cited works, the unknown deformations and thus, wrinkles or slacks, follow directly from an energy minimization principle. However, if wrinkles are modeled explicitly, a large number of finite elements is required in order to capture the respective deformation adequately. Hence, the numerical effort associated with this modeling strategy is relatively high compared to the approaches described in the previous paragraph. Consequently, they will not be considered in the remaining part of this paper.

Neglecting bending stiffness, a variational strategy similar to that in [11, 12] was proposed in a series of papers by Pipkin, cf. [13–15]. In [13], Pipkin analyzed the energy of a membrane for isotropic hyperelastic material models. He proved that the quasi-convexification of the Helmholtz energy which guarantees, under a few further conditions, lower semi-continuity of the resulting potential of the considered mechanical system and hence, the existence of solutions (energy minimizers; see [16]), defines a relaxed energy functional whose derivatives yield the membrane stresses. More precisely, the stresses predicted by this relaxed potential obey the restrictions imposed by tension field theory, i.e., the resulting stress field is associated with uniaxial tension. Pipkin further elaborated his ideas in [15]. In this work, he analyzed wrinkling in arbitrary anisotropic hyperelastic solids. Under the assumption that the two-dimensional Helmholtz energy of the membrane is convex (with respect to the right Cauchy-Green tensor), Pipkin generalized his findings for isotropic material models to arbitrary symmetries. Pipkin's method allows to re-formulate tension field theory within a variational framework. It should be noted that a different approach leading to similar results was proposed by Epstein [17].

Surprisingly, although Pipkin's ideas are well-suited for algorithmic formulations, a fully variational numerical framework has not been advocated yet. As a consequence, within the present paper, the ideas by Pipkin are further elaborated and implemented in a finite element code resulting in a numerically efficient formulation. In the context of three-dimensional hyperelasto-(visco)plasticity, a similar variational framework was proposed by Ortiz and co-workers [18–20] (see also the more recent works [21, 22]). Roughly speaking, in those approaches which are often referred to as *variational constitutive updates* the state variables follow from relaxing a certain potential. Based on this relaxed functional, the deformation mapping results from energy minimization as well. In the present paper, a similar numerical strategy for the analysis of wrinkles and slacks in arbitrary hyperelastic membranes at finite strains is discussed. In contrast to the works by Pipkin, the non-vanishing out-of-plane component of the strain tensor is considered and follows from energy relaxation as well. Consequently, plane stress conditions do not need to be enforced explicitly but are naturally included within the novel variational framework. As a result, three-dimensional constitutive models can be directly applied without any modification required. Furthermore, since within the proposed variational method all unknown state variables and the deformation mapping follow from a minimization principle, standard optimization strategies can be adopted for solving the resulting mechanical problem. This is especially important for highly non-linear or singular problems such as wrinkling. An additional appealing property of minimization principles is that they provide a natural basis to estimate the quality of the numerical solution and hence, they represent a natural basis

for mesh adaption, cf. [23–25]. As a prototype, a variational h -adaption is discussed within the presented paper.

The paper is organized as follows: In Section 2, the kinematics of wrinkles and slacks are discussed. Based on an intuitive engineering approach it is shown that most of the different models which can be found in the literature are essentially equivalent. A novel algorithmic formulation for wrinkling representing one of the key contributions of the present paper is shown in Section 3. Starting with the fundamentals, criteria signaling the formation of wrinkles and slacks are derived. In case of wrinkling, the respective state variables are computed from a local minimization principle. All linearizations required for applying an optimization strategy such as Newton’s method are given. Section 4 is concerned with a novel variational h -adaption for membranes. Using the variational structure of the underlying mechanical problem, a physically and mathematically sound error indicator is proposed. Finally, the applicability and versatility of the variational wrinkling algorithm as well as the performance of the novel variational h -adaption for membranes are illustrated by means of two numerical examples in Section 5.

2 Kinematics of wrinkling

In this section, the kinematics of wrinkling are discussed. Although different models can be found in the literature, it will be shown that they are essentially equivalent. More precisely, they are included within a general framework proposed by Pipkin [15]. However, since Pipkin’s approach is based on a rather mathematical argumentation such as quasi-convexification, an intuitive engineering wrinkling model is presented in Section 2.1 first. Subsequently, it is modified finally resulting in Pipkin’s method. In Section 2.2, the kinematics are slightly enhanced such that they account for a non-vanishing out-of-plane strain component. This is necessary in order to employ three-dimensional constitutive models.

2.1 Fundamentals

In what follows, a membrane occupying a region $\Omega \in \mathbb{R}^3$ in its reference undeformed configuration is considered. Since a membrane represents a two-dimensional submanifold in \mathbb{R}^3 , it can be conveniently characterized (at least locally) by a chart $\tilde{\mathbf{X}} : \mathbb{R}^2 \supset \mathcal{U} \rightarrow \mathcal{M} \subset \mathbb{R}^3$, $\theta_\alpha \mapsto \mathbf{X}$ implying the introduction of curvilinear coordinates θ_1, θ_2 . The same holds for the deformed configuration, i.e., $\tilde{\mathbf{x}} : \mathbb{R}^2 \supset \mathcal{U} \rightarrow \mathcal{K} \subset \mathbb{R}^3$, $\theta_\alpha \mapsto \mathbf{x}$. Here, \mathbf{X} , \mathbf{x} denote position vectors of a point within the undeformed and the deformed configuration, respectively. With these charts which are sufficiently smooth diffeomorphisms, i.e., $\tilde{\mathbf{X}} \in \text{Diff}^1(\mathcal{U}, \mathcal{M})$ and $\tilde{\mathbf{x}} \in \text{Diff}^1(\mathcal{U}, \mathcal{K})$, the deformation mapping connecting \mathbf{X} and \mathbf{x} is well defined, i.e., $\varphi = \tilde{\mathbf{x}} \circ \tilde{\mathbf{X}}^{-1}$. Locally, the deformation is measured by the deformation gradient $\mathbf{F} := \partial \tilde{\mathbf{x}} / \partial \theta_\alpha \otimes \partial \theta_\alpha / \partial \tilde{\mathbf{X}}$. Based on \mathbf{F} strain measures can be derived. One such measure is the right Cauchy-Green tensor $\mathbf{C} = \mathbf{F}^T \cdot \mathbf{F}$ represented by a symmetric and positive definite second-order tensor. It bears emphasis that without loss of generality, the deformation gradient \mathbf{F} as well as the strain tensor \mathbf{C} are defined by 2×2 tensors within this subsection, even if a three-dimensional space is considered. Further comments are omitted, cf. [14, 26]. In the remaining part of this paper the notation $\mathbf{C} > 0$ is used to signal that \mathbf{C} is positive definite.

Next, focus is on a modified strain tensor reflecting effects due to wrinkling. According to Roddeman et al. [3], wrinkles can be taken into account by modifying the deformation gradient. More precisely, following [3, 4], the standard deformation gradient \mathbf{F} is enhanced multiplicatively resulting in a relaxed deformation gradient \mathbf{F}_r , i.e.,

$$\mathbf{F}_r = (\mathbf{1} + \tilde{a} \mathbf{n} \otimes \mathbf{n}) \cdot \mathbf{F}, \quad \tilde{a} \geq 0 \quad (1)$$

Here, \mathbf{n} is the wrinkle direction and \tilde{a} the local change in length of the membrane due to wrinkling. Subsequently, the material response is computed by using \mathbf{F}_r instead of \mathbf{F} . It bears emphasis that Eq. (1) is formally identical to the well-known split in multiplicative plasticity theory ($\mathbf{F} = \mathbf{F}^e \cdot \mathbf{F}^p$). This can be seen better by applying the Sherman-Morrison formula, i.e.,

$$\mathbf{F} = \mathbf{F}_w \cdot \mathbf{F}_r, \quad \mathbf{F}_w = \mathbf{1} - \frac{\tilde{a}}{1 + \tilde{a}} \mathbf{n} \otimes \mathbf{n} \quad (2)$$

Although both models look identical, it should be noted that they are significantly different. While plasticity is history-dependent and thus path-dependent, wrinkling can be computed locally (in space and time).

By the principle of material objectivity, the material response depends on \mathbf{F}_r through the respective right Cauchy-Green tensor. From Eq. (1) \mathbf{C}_r it is obtained as

$$\mathbf{C}_r := \mathbf{F}_r^T \cdot \mathbf{F}_r = \mathbf{F}^T \cdot \mathbf{F} + [2\tilde{a} + \tilde{a}^2] (\mathbf{n} \cdot \mathbf{F}) \otimes (\mathbf{n} \cdot \mathbf{F}) \quad (3)$$

Consequently, by setting

$$a^2 := (2\tilde{a} + \tilde{a}^2) \|\mathbf{n} \cdot \mathbf{F}\|_2^2 \geq 0, \quad \mathbf{N} = \frac{\mathbf{n} \cdot \mathbf{F}}{\|\mathbf{n} \cdot \mathbf{F}\|_2} \quad (4)$$

Eq. (3) can be re-written as

$$\mathbf{C}_r = \mathbf{C} + \mathbf{C}_w, \quad \mathbf{C}_w = a^2 \mathbf{N} \otimes \mathbf{N} \quad (5)$$

Hence, the additive enhancement of the right Cauchy-Green tensor (5) is equivalent to the multiplicative split $\mathbf{F} = \mathbf{F}_r \cdot \mathbf{F}_w$.

Clearly, Roddeman's model, or equivalently the split (5), are associated with the kinematics induced by wrinkling. However, in the present paper, wrinkles as well as slacks are to be modeled. Hence, a slight modification of the kinematics is proposed, i.e, an additive decomposition of the Cauchy-Green tensor according to

$$\mathbf{C}_r = \mathbf{C} + \mathbf{C}_w, \quad \mathbf{C}_w = a^2 \mathbf{N} \otimes \mathbf{N} + b^2 \mathbf{M} \otimes \mathbf{M} \quad (6)$$

is adopted. Here, \mathbf{N} and \mathbf{M} span a cartesian coordinate system. Obviously, \mathbf{C}_w is identical to Eq. (5), if b equals zero. Otherwise, \mathbf{C}_w corresponds to a slack. This will be shown in the next sections.

According to the spectral decomposition theorem, any symmetric tensor which is semi-positive definite can be re-written into a format such as Eq. (6)₂. In the following, the notation $\mathbf{C}_w \geq 0$ is used to indicate that \mathbf{C}_w is represented by a semi positive definite tensor. For this reason, Eq. (6) is equivalent to

$$\mathbf{C}_r = \mathbf{C} + \mathbf{C}_w, \quad \mathbf{C}_w \geq 0 \quad (7)$$

which has been proposed by Pipkin, cf. [15].

Remark 1. It bears emphasis that wrinkling is treated as a purely local problem within this paper. More precisely, in line with plasticity theory, the wrinkling parameters (a, α) defining the enhanced kinematics according to Eq. (1) or (5) are incompatible, i.e., they do not derive from a compatible displacement field. Thus, they are not continuous in general. However, it is obvious that continuity can easily be enforced.

Remark 2. Similar to Roddeman, Epstein [17] proposed modified kinematics of the type

$$\mathbf{F}_r = \widehat{\mathbf{F}}^{-1} \cdot \mathbf{F}, \quad \widehat{\mathbf{F}} := \mathbf{Q} \cdot [\exp(-\alpha^2) \mathbf{n} \otimes \mathbf{n} + \mathbf{m} \otimes \mathbf{m}], \quad \alpha \in [0, \infty) \quad (8)$$

Here, \mathbf{n} and \mathbf{m} are defined as before, $\mathbf{Q} \in SO(2)$ is an arbitrary proper orthogonal tensor and α is, as will be seen, associated with the change in length of the membrane due to wrinkling. Without loss of generality, $\mathbf{Q} = \mathbf{1}$ is considered in what follows (\mathbf{Q} does not affect \mathbf{C}). Clearly, by using $\mathbf{n} \otimes \mathbf{n} + \mathbf{m} \otimes \mathbf{m} = \mathbf{1}$, $\widehat{\mathbf{F}}$ can be re-written as

$$\widehat{\mathbf{F}} = \mathbf{1} + \underbrace{[\exp(-\alpha^2) - 1]}_{=: \tilde{\alpha}} \mathbf{n} \otimes \mathbf{n} \quad (9)$$

and finally, application of the Sherman-Morrison formula yields

$$\widehat{\mathbf{F}}^{-1} = \mathbf{1} - \frac{\tilde{\alpha}}{1 + \tilde{\alpha}} \mathbf{n} \otimes \mathbf{n} \quad (10)$$

Hence, by setting

$$\tilde{a} := -\frac{\tilde{\alpha}}{1 + \tilde{\alpha}} \geq 0 \quad (11)$$

Epstein's assumption is equivalent to Roddeman's model.

2.2 Modification of the kinematics required for applying three-dimensional constitutive models

Clearly, if a fully three-dimensional material model is to be used, the plane stress condition characterizing a membrane cannot be guaranteed a priori. As a consequence, the kinematics have to be slightly modified. In what follows, the vector \mathbf{E}_3 is defined by $\mathbf{E}_3 := \mathbf{N} \times \mathbf{M}$. With this definition, the two-dimensional relaxed strain tensor \mathbf{C}_r in Eq. (7) is replaced by

$$\mathbf{C}_r = \mathbf{C} + \mathbf{C}_w + C_{33} \mathbf{E}_3 \otimes \mathbf{E}_3, \quad \mathbf{C}_w \geq 0, \quad C_{33} > 0 \quad (12)$$

In contrast to Eq. (7), all tensors in Eq. (12) belong to $\mathbb{R}^{3 \times 3}$. More precisely, \mathbf{C} as well as \mathbf{C}_w in Eq. (12) are obtained by adding additional zeros to the respective tensors in Eq. (7). The generally non-vanishing component C_{33} can be computed from the plane stress condition or as will be shown in this paper, from relaxing an energy potential.

Remark 3. Not every hyperelastic three-dimensional constitutive model can be used. More specifically, it has to fulfill some material symmetry conditions, i.e., the shear components $(\bullet)_{i3}$ of the stresses resulting from \mathbf{C}_r as defined in Eq. (12) have to vanish. Obviously, isotropic models fulfill this restriction.

3 A novel wrinkling algorithm based on energy minimization

In this section, a novel wrinkling algorithm is discussed. In contrast to other implementations which can be found in the literature, it is based on energy minimization. More precisely, the ideas proposed Pipkin by [15] are further elaborated and implemented resulting in an efficient finite element code. One of the distinguishing features of the resulting method is that the principle of energy minimization, together with the kinematics (5) define the formation of wrinkles and slacks completely. Consequently, and in contrast to other numerical approaches, additional

assumptions such as those of tension field theory do not have to be enforced explicitly, but are naturally included.

The fundamentals of the algorithmic formulation are discussed in Subsection 3.1 first. For the sake of clarity, attention is focused on anisotropic hyperelastic material models which fulfill a priori plane stress conditions. Criteria associated with the formation of slacks and wrinkles are elaborated in Subsection 3.2, while details about the numerical implementation are shown in Subsection 3.3. Finally, Subsection 3.4 is concerned the modifications of the numerical implementation necessary for applying three-dimensional constitutive models directly.

3.1 Fundamentals

As mentioned before, for the sake of clarity, attention is focused first on anisotropic hyperelastic material models which fulfill a priori plane stress conditions. Such a model is described in the appendix of this paper. Hence, in what follows, $\mathbf{C} \in \mathbb{R}^{2 \times 2}$. The respective generalizations will be discussed in Subsection 3.4.

With the strain energy density $\Psi(\mathbf{C}) \geq 0$, the first Piola-Kirchhoff stress tensor \mathbf{P} and the second Piola-Kirchhoff stresses \mathbf{S} are computed as

$$\mathbf{P} = 2 \mathbf{F} \cdot \frac{\partial \Psi}{\partial \mathbf{C}} \quad \mathbf{S} = 2 \frac{\partial \Psi}{\partial \mathbf{C}} \quad (13)$$

Furthermore, it is assumed that the reference configuration is fully unloaded (locally), i.e.,

$$\Psi(\mathbf{C} = \mathbf{1}) = 0, \quad \mathbf{P}(\mathbf{C} = \mathbf{1}) = \mathbf{0} \quad (14)$$

It is well known that for such material models the deformation mapping φ can be computed by applying the principle of minimum potential energy. This can be written as

$$\varphi = \arg \inf_{\varphi} I(\varphi), \quad (15)$$

with

$$I(\varphi) := \int_{\Omega} \Psi(\mathbf{C}) \, dV - \int_{\Omega} \mathbf{B} \cdot \varphi \, dV - \int_{\partial\Omega_2} \bar{\mathbf{T}} \cdot \varphi \, dA. \quad (16)$$

Here, \mathbf{B} and $\bar{\mathbf{T}}$ represent prescribed body forces and tractions acting at $\partial\Omega_2$. Obviously, φ has to comply with the essential boundary conditions imposing additional restrictions in the resulting minimization problem. Clearly, if principle (15) is directly employed, compressive stresses violating the physical properties of membranes may occur.

Following Section 2, wrinkles and slacks can be taken into account by replacing the standard Cauchy-Green tensor by its relaxed counterpart

$$\mathbf{C}_r := \mathbf{C} + a^2 \mathbf{N} \otimes \mathbf{N} + b^2 \mathbf{M} \otimes \mathbf{M}, \quad a^2, b^2 \geq 0 \quad (17)$$

Since energy minimization is the overriding principle governing every aspect of the mechanical problem under investigation, it is natural to postulate that wrinkles and slacks form such that they lead to the energetically most favorable state. Hence, the modified principle of minimum potential energy

$$(\varphi, a^2, b^2, \alpha) = \arg \inf_{\varphi, a^2, b^2, \alpha} I(\varphi), \quad (18)$$

with

$$I(\varphi, a^2, b^2, \alpha) := \int_{\Omega} \Psi(\mathbf{C}_r) \, dV - \int_{\Omega} \mathbf{B} \cdot \varphi \, dV - \int_{\partial\Omega_2} \bar{\mathbf{T}} \cdot \varphi \, dA \quad (19)$$

and the parameterization

$$\mathbf{N} = [\cos \alpha; \sin \alpha], \quad \mathbf{M} = [-\sin \alpha; \cos \alpha] = \partial_\alpha \mathbf{N} \quad (20)$$

is considered. In the remaining part of this section it will be shown how to determine efficiently the wrinkling (slack) parameters a^2 , b^2 and α , together with the deformation mapping φ based on Eq. (18). Furthermore, the implications resulting from this variational principle are discussed.

Since the wrinkling variables (a^2 , b^2 and α) are defined locally, the minimization problem (18) can be decomposed into two classes of optimization problems. First, for a given deformation mapping, the parameters a^2 , b^2 and α are computed from the local minimization principle

$$(a^2, b^2, \alpha) := \arg \inf_{\substack{a^2 > 0 \\ b^2 > 0 \\ \alpha \in [0, \pi]}} \Psi(\mathbf{C}_r), \quad (21)$$

Clearly, this in turn, defines a relaxed energy functional

$$\Psi_r(\mathbf{C}) := \inf_{\substack{a^2 > 0 \\ b^2 > 0 \\ \alpha \in [0, \pi]}} \Psi(\mathbf{C}_r), \quad (22)$$

depending only on the deformation mapping. Interestingly, Eq. (22) is formally identical to so-called variational constitutive updates such as proposed by Ortiz et al., cf. [18, 19].

Once the local problem (22) has been solved, the deformation mapping follows from

$$\varphi = \arg \inf_{\varphi} \left[\int_{\Omega} \Psi_r(\mathbf{C}) \, dV - \int_{\Omega} \mathbf{B} \cdot \varphi \, dV - \int_{\partial\Omega_2} \bar{\mathbf{T}} \cdot \varphi \, dA \right] \quad (23)$$

It bears emphasis that both problems (21) and (23) can be computed by using standard optimization algorithms. Clearly, a spatial discretization of Eq. (23) is required. The applicability of standard numerical methods is a very appealing feature of the proposed framework, since wrinkling leads usually to highly nonlinear and singular system of equations.

Problem (23) can be treated as standard hyperelasticity. Consequently, focus is on the solution of Eq. (21) in the remaining part of this section. Although for some classes of hyperelastic material models closed form solutions for the relaxed energy can be derived, cf. [13, 27], numerical methods are required in general.

Remark 4. It is noteworthy that minimization principle (21) is smooth in a , b and α (if Ψ is smooth in \mathbf{C}). As a consequence, the transition between the classical solution ($a = b = 0$) and wrinkles or slacks is smooth for the variational strategy. This improves the numerical robustness of the resulting finite element method significantly.

3.2 Wrinkling criteria

In principle, optimization problem (22) could be implemented directly. However, such a formulation is not very efficient. For instance, consider a loading state which does not lead to wrinkling. In such a case, it is more convenient to derive a criterion signalling in advance that wrinkles will not occur. Referring to computational plasticity or variational constitutive updates a so-called trial step is usually applied. In the next paragraphs, analogous criteria will be derived.

3.2.1 Formation of slacks

In this subsection, criteria necessary for the formation of slacks are discussed. Here and henceforth, a slack is defined by a relaxed Cauchy-Green tensor showing non-vanishing wrinkling parameters in both directions, i.e., $a^2 > 0$ and $b^2 > 0$. This definition coincides with those which can be found in the literature. In this case, the stationarity conditions associated with Eq.(21) yield

$$\begin{aligned} \frac{\partial \Psi}{\partial \mathbf{C}_r} : \frac{\partial \mathbf{C}_r}{\partial a} &= 0 \\ \Leftrightarrow a \mathbf{S} : (\mathbf{N} \otimes \mathbf{N}) &= 0 \end{aligned} \quad (24)$$

$$\begin{aligned} \frac{\partial \Psi}{\partial \mathbf{C}_r} : \frac{\partial \mathbf{C}_r}{\partial b} &= 0 \\ \Leftrightarrow b \mathbf{S} : (\mathbf{M} \otimes \mathbf{M}) &= 0 \end{aligned} \quad (25)$$

$$\begin{aligned} \frac{\partial \Psi}{\partial \mathbf{C}_r} : \frac{\partial \mathbf{C}_r}{\partial \alpha} &= 0 \\ \Leftrightarrow [a^2 - b^2] \mathbf{S} : (\mathbf{N} \otimes \mathbf{M}) &= 0 \end{aligned} \quad (26)$$

Since \mathbf{S} belongs to the space of symmetric second order tensors which can be generated by $\mathbb{S} = \text{span}\{\mathbf{N} \otimes \mathbf{N}, \mathbf{M} \otimes \mathbf{M}, (\mathbf{N} \otimes \mathbf{M})^{\text{sym}}\}$, Eqs. (24)-(26) imply that slacks are stress free, i.e., $\mathbf{S} = \mathbf{0}$ (the case $b = a$ does not lead to any problems as will be shown in the next paragraph). Thus, if additionally, the physically sound conditions $\mathbf{S}(\mathbf{C}) = \mathbf{0} \Leftrightarrow \mathbf{C} = \mathbf{1}$ and $\Psi(\mathbf{C}) = 0 \Leftrightarrow \mathbf{C} = \mathbf{1}$ are assumed, a slack is represented by

$$\text{slack} \iff a^2 > 0, b^2 > 0, \mathbf{C}_r = \mathbf{1} \quad (27)$$

The aforementioned assumptions are closely related to the *Generalized Coleman-Noll Inequality*, cf. [28].

Next, the conditions associated with the formation of slacks are discussed. For that purpose, the spectral decomposition of the compatible Cauchy-Green tensor is considered, i.e.,

$$\mathbf{C} = \sum_{i=1}^2 \lambda_i^2 \tilde{\mathbf{N}}_i \otimes \tilde{\mathbf{N}}_i \quad (28)$$

Suppose this \mathbf{C} results in a slack. In this case, the wrinkling-related part of the relaxed Cauchy-Green tensor is given by

$$\mathbf{C}_r = \mathbf{1} \implies \mathbf{C}_w = \sum_{i=1}^2 (1 - \lambda_i^2) \tilde{\mathbf{N}}_i \otimes \tilde{\mathbf{N}}_i \quad (29)$$

Since \mathbf{C}_w is a positive definite tensor in case of slacks ($a^2 > 0, b^2 > 0$), the eigenvalues of \mathbf{C} have to fulfill

$$\lambda_i^2 < 1 \quad (30)$$

That is, slacks can only form if the strains are of purely compressive type. Thus, in summary, the following implications hold

$$\boxed{\lambda_1^2 < 1, \lambda_2^2 < 1 \implies \text{slack} \implies \mathbf{C}_r = \mathbf{1}, \implies \mathbf{S} = \mathbf{0}, \Psi = 0} \quad (31)$$

This condition is equivalent to that known from the classical strain-based or strain-stress-based wrinkle criteria, cf. [6, 7]. It is noteworthy that within the proposed variational framework, the criterion associated with the formations of slacks follows naturally from energy minimization and does not have to be enforced in an ad-hoc manner.

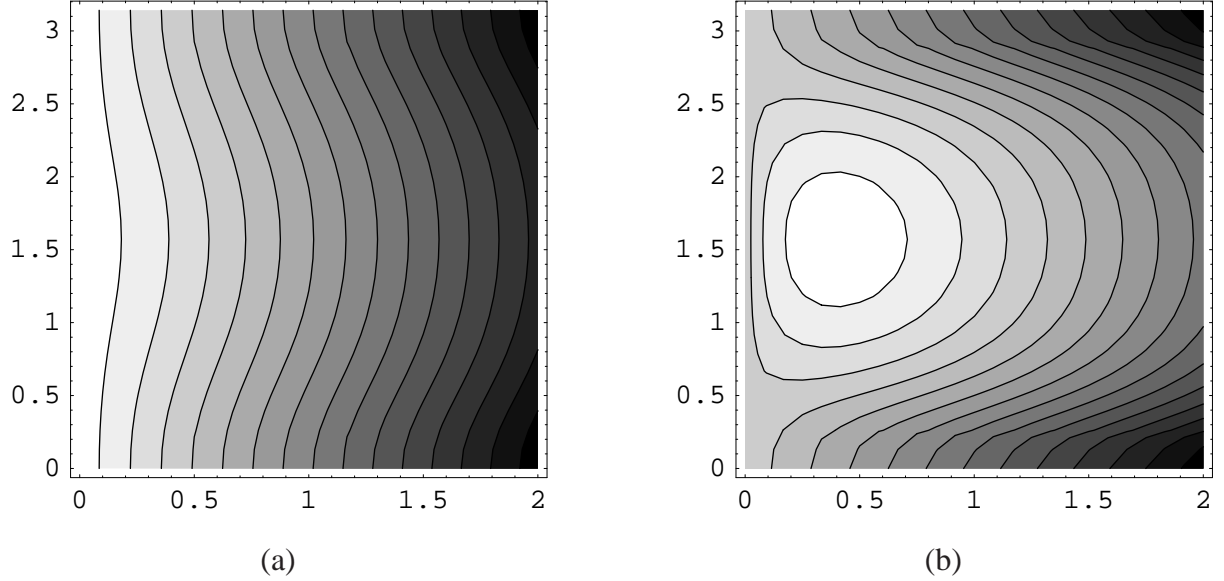


Figure 1: Energy landscape of $\Psi(\mathbf{C}_r(a^2, \alpha))$ as a function in a (horizontal direction) and α (vertical direction); a minimum is highlighted by white color. The respective isotropic stored energy functional is given in Appendix A. Plots for: (a) a compatible Cauchy-Green tensor $\mathbf{C} = \text{diag}\{2; 0.9\}$; the minimum is associated with $a^2 = 0$ implying that no wrinkles will occur. (b) $\mathbf{C} = \text{diag}\{2; 0.5\}$; minimum occurs at $a^2 > 0$ and \mathbf{N} points into the direction of the smaller eigenvalue of \mathbf{C} , i.e., $\alpha = \pi/2$. Hence, a wrinkle will form.

3.2.2 Formation of wrinkles

Analogously to the previous subsection, wrinkling is defined by a relaxed Cauchy-Green tensor showing only one non-vanishing wrinkling parameter ($a^2 > 0$, $b^2 = 0$). In this case, the stationarity conditions of Eq.(21) are obtained as (cf. Eqs. (24)-(26))

$$\begin{aligned} \mathbf{S} : (\mathbf{N} \otimes \mathbf{N}) &= 0 \\ \mathbf{S} : (\mathbf{N} \otimes \mathbf{M}) &= 0 \end{aligned} \quad \Leftrightarrow \quad \mathbf{S} \cdot \mathbf{N} = 0 \quad (32)$$

As a consequence, wrinkles are characterized by a uniaxial stress state. This condition known from tension field theory, cf. [8], is usually enforced explicitly. It bears emphasis that within the variational model it is naturally included.

For the derivation of necessary and sufficient conditions associated with wrinkling, the energy

$$\Psi(\mathbf{C}_r) = \Psi(\mathbf{C}_r(\mathbf{C}, a, \alpha)) \quad (33)$$

as a function in a and α is analyzed (for constant \mathbf{C}), see Fig. 1. Wrinkles do not occur, if the solution is optimal (stable) from an energetical point of view, i.e., if

$$(0, \alpha) = \arg \inf_{\substack{a^2 \geq 0 \\ \alpha \in [0, \pi]}} \Psi(\mathbf{C}_r), \quad \mathbf{C}_r = \mathbf{C} + a^2 \mathbf{N} \otimes \mathbf{N} \quad (34)$$

Otherwise wrinkles form resulting in a reduction of the energy. Obviously,

$$\Psi(\mathbf{C}_r(a=0), \alpha) = \Psi(\mathbf{C}) \quad (35)$$

and furthermore, according to Eqs. (24) and (26),

$$[\partial_a \Psi(\mathbf{C}_r); \partial_\alpha \Psi(\mathbf{C}_r)]|_{a=0} = \mathbf{0} \quad (36)$$

Hence, the classical solution ($a = 0$) is associated with a saddle point (in the a - α diagram). For the derivation of wrinkling conditions, stability of the standard solution ($a = 0$) is studied. This can be done by analyzing the second derivative

$$\partial_a^2 \Psi = \mathbf{S} : (\mathbf{N} \otimes \mathbf{N}) + a^2 (\mathbf{N} \otimes \mathbf{N}) : \mathbb{C} : (\mathbf{N} \otimes \mathbf{N}), \quad \mathbb{C} := 4 \frac{\partial \Psi^2}{\partial \mathbf{C}_r^2} \quad (37)$$

Hence, for $a = 0$,

$$\partial_a^2 \Psi|_{a=0} = \mathbf{S} : (\mathbf{N} \otimes \mathbf{N}) \quad (38)$$

is obtained. Consequently, stability in an energetical sense requires the minimal eigenvalue to be greater than zero. If one of the eigenvalues is less than zero wrinkles form (or slacks). This is equivalent to the classical (ad-hoc) theory. Thus, in summary, the following wrinkling condition holds

$$\boxed{\lambda_1^2 > 1, \lambda_2^2 < \lambda_1^2, \mathbf{S}(\mathbf{C}) \not\geq 0 \Rightarrow \text{wrinkling} \Rightarrow (a^2, \alpha) \text{ see Eq. (21)}} \quad (39)$$

Remark 5. As mentioned before, within many membrane models, the wrinkling parameters a and α are computed by applying tension field theory [8]. Consequently, a and α are obtained from the non-linear set of equations

$$\mathbf{R}_S := \mathbf{S} \cdot \mathbf{N} = \mathbf{0} \quad (40)$$

With $\mathbf{a} := (a, \alpha)$, Eq. (40) defines an implicit function of the type (under some mathematical restrictions)

$$\mathbf{a} = \mathbf{f}(\mathbf{C}) \quad (41)$$

and thus,

$$\mathbf{C}_r = \mathbf{g}(\mathbf{C}) \quad (42)$$

cf. [17]. With this implicitly defined function \mathbf{g} , a relaxed stored energy functional can be defined, i.e.,

$$\Psi_r(\mathbf{C}) = \Psi \circ \mathbf{g}(\mathbf{C}) \quad (43)$$

As a consequence, the kinematical approach $\mathbf{C}_r = \mathbf{C} + \mathbf{C}_w$ is equivalent to modifying the stored energy functional, cf. [7].

Remark 6. Clearly, Eqs. (32) imply that the wrinkling tensor \mathbf{C}_w is coaxial to \mathbf{S} . Consequently, if the Helmholtz energy is isotropic in \mathbf{C} , \mathbf{C}_w is coaxial to \mathbf{C} as well. Hence, for isotropic material models, the vector \mathbf{N} , or equivalently α , is known in advance. As a result, only the wrinkling parameter a has to be computed numerically which improves the algorithmic efficiency significantly.

3.2.3 Stable solution without wrinkles or slacks

According to the previous subsection, the classical solution is stable from an energetical point of view, if the stresses are (semi-) positive definite. Hence, the following condition can be derived

$$\boxed{\mathbf{S} \geq 0 \Rightarrow \text{no wrinkles or slacks}} \quad (44)$$

3.3 Numerical implementation of energy-driven wrinkling

Details about the numerical implementation are discussed within this subsection. In contrast to most works previously published, the proposed algorithm is directly based on the underlying variational principle governing the formation of wrinkles or slacks. More precisely, the local state variables are computed by minimizing the respective Helmholtz energy.

Following Subsections 3.2.1 - 3.2.3, the local state of a membrane undergoing large deformations can be classified into the following groups: wrinkles, slacks and the classical solution without any wrinkles or slacks. To identify the type of a given deformation, the largest eigenvalue of the compatible right Cauchy-Green tensor \mathbf{C} is computed first. Subsequently, the criterion signalling the formation of slacks (31) is checked. In case of slacks, the wrinkling-related part of the Cauchy-Green tensor follows directly from a spectral decomposition, cf. Eq. (29). On the other hand, if the largest eigenvalue of \mathbf{C} is greater than one, the possibility of wrinkling has to be analyzed. For that purpose, the smallest eigenvalue of the stress tensor is calculated by assuming a trial state characterized by $\mathbf{C}_w = \mathbf{0}$. If this value is greater than zero, no wrinkles or slacks will form and the trial state represents already the solution to the problem. On the other hand, if inequality (44) does not hold, the standard solution ($\mathbf{C}_w = \mathbf{0}$) has to be relaxed and the wrinkling strains are computed from the minimization problem (21) with $b^2 = 0$.

It should be noted that for isotropic models, the classification of the type of deformation can be implemented more efficiently. For instance, as stated in [28], if the considered (standard) hyperelastic material obeys the strong ellipticity condition, it fulfills the Baker-Ericksen inequalities. These inequalities in turn imply that the greater principal stress occurs always in the direction of the greater principal stretch. Hence, the smaller principal stress can be computed directly without calculating all components of the stress tensor.

Clearly, the classical solution (no wrinkles or slacks) does not require any modification of the standard hyperelastic constitutive model. Likewise, in case of slacks, the computation of the wrinkling strains is straightforward. Hence, the only non-trivial problem is the calculation of the mechanical response, if wrinkles occur. As mentioned before, classical optimization algorithms can be applied to solve the respective minimization problem (21). We have employed three different optimization schemes: a conjugate gradient algorithm of Fletcher-Reeves and Polak-Ribiere type [29], a limited memory BFGS method [30] and a damped Newton's scheme, cf. [31] for further details. Since for each of those methods the derivatives of the function to be minimized are required, they are summarized within the next paragraphs.

3.3.1 First derivatives – Residuals

In case of wrinkling, the non-linear set of equations (21) has to be solved for $b = 0$. The respective stationarity condition reads, cf. Subsection 3.2.2,

$$\mathbf{R}_S(\mathbf{a}) = \mathbf{0}, \quad \mathbf{a} := [a^2; \alpha]^T \quad (45)$$

or equivalently,

$$\mathbf{R}_P(\mathbf{a}) = \mathbf{0}, \quad \mathbf{a} := [a^2; \alpha]^T \quad (46)$$

with the first derivatives given by

$$\mathbf{R}_S(\mathbf{a}) := \mathbf{S}(a^2, \alpha) \cdot \mathbf{N}(\alpha), \quad \mathbf{R}_P(\mathbf{a}) := \mathbf{P}(a^2, \alpha) \cdot \mathbf{N}(\alpha) \quad (47)$$

It should be noted that, the deformation gradient \mathbf{F} is regular and hence, $\mathbf{R}_S(\mathbf{a}) = \mathbf{0}$ or $\mathbf{R}_P(\mathbf{a}) = \mathbf{0}$ is indeed equivalent to vanishing 'true' stresses, i.e., $\boldsymbol{\sigma} \cdot \mathbf{n} = \mathbf{0}$. Here, $\boldsymbol{\sigma}$ denotes the Cauchy stresses.

3.3.2 Second derivatives

If Newton's method is to be applied, the second derivatives are required as well. The linearizations of Eq. (45) are given by (for fixed \mathbf{C})

$$\frac{\partial \mathbf{R}_S}{\partial(a^2)} = \frac{1}{2} \mathbf{N} \cdot \mathbb{C} : (\mathbf{N} \otimes \mathbf{N}), \quad \mathbb{C} := 4 \frac{\partial \Psi^2}{\partial \mathbf{C}_r^2} \quad (48)$$

$$\frac{\partial \mathbf{R}_S}{\partial \alpha} = \mathbf{S} \cdot \mathbf{M} + \frac{1}{2} a^2 \mathbf{N} \cdot \mathbb{C} : \partial_\alpha (\mathbf{N} \otimes \mathbf{N}) \quad (49)$$

3.3.3 Consistent linearization - algorithmic tangent moduli

Suppose Newton's method is adopted to solve the resulting global minimization problem (23). In this case, the linearization of the considered optimization algorithm is required to guarantee an asymptotical quadratic convergent. Assuming the (local) wrinkling problem is converged, the linearizations of Eq. (45) can be calculated (\mathbf{C} is not fixed anymore). A straightforward calculation yields

$$d\mathbf{a} = -\frac{1}{2} (\partial_{(a^2)} \mathbf{R}_S \mid \partial_\alpha \mathbf{R}_S)^{-1} \cdot (\mathbf{N} \cdot \mathbb{C}) : d\mathbf{C}, \quad \mathbf{a} = [a^2; \alpha] \quad (50)$$

For the sake of compactness, the third-order tensor \mathcal{A} is introduced by

$$d\mathbf{a} = \mathcal{A} : d\mathbf{C}. \quad (51)$$

With this notation, the consistent tangent can be computed by

$$\mathbb{C}_T := 2 \frac{d\mathbf{S}}{d\mathbf{C}} = \mathbb{C} : [\mathbb{I}^{\text{sym}} + (\mathbf{N} \otimes \mathbf{N}) \otimes \mathcal{A}^{(1)} + 2 a^2 (\mathbf{N} \otimes \mathbf{M}) \otimes \mathcal{A}^{(2)}] \quad (52)$$

Here, the tensors $\mathcal{A}^{(i)}$ are defined according to

$$[\mathcal{A}^{(i)}]_{jk} = [\mathcal{A}]_{ijk}, \quad (53)$$

Clearly, by using the identity

$$\mathbf{P} = d_{\mathbf{F}} \Psi = \partial_{\mathbf{C}_r} \Psi : d_{\mathbf{C}} \mathbf{C}_r : \partial_{\mathbf{F}} \mathbf{C} = \mathbf{F} \cdot \mathbf{S} \quad (54)$$

the linearizations of the first Piola-Kirchhoff stresses can be computed as well. They result in

$$\mathbb{A} := \frac{d\mathbf{P}}{d\mathbf{F}} = \mathbf{1} \overline{\otimes} \mathbf{S} + [\mathbf{F} \cdot \mathbb{C}_T \cdot \mathbf{F}^T]^t, \quad \text{with } [\mathbb{P}^t]_{ijkl} = [\mathbb{P}]_{ijlk}. \quad (55)$$

The non-standard dyadic product $\overline{\otimes}$ is defined in Appendix A.1.

3.4 Modification of the numerical implementation for applying three-dimensional constitutive models

According to Subsection 2.2, if a fully three-dimensional material model is to be used, the plane stress condition characterizing a membrane cannot be guaranteed a priori. As a consequence, the kinematics have to be slightly modified, i.e.,

$$\mathbf{C}_r = \mathbf{C} + \mathbf{C}_w + C_{33} \mathbf{E}_3 \otimes \mathbf{E}_3, \quad \mathbf{C}_w \geq 0, \quad C_{33} > 0 \quad (56)$$

Hence, instead of Eq. (21) the modified minimization principle reads now

$$(C_{33}, a^2, b^2, \alpha) := \arg \inf_{\substack{C_{33} > 0 \\ a^2 \geq 0 \\ b^2 \geq 0 \\ \alpha \in [0, \pi]}} \Psi(\mathbf{C}_r), \quad (57)$$

This can be shown as follows. First, it is noted that the stationarity conditions with respect to a , b and α are not affected by the modified kinematics. Hence, they are identical to those described in detail in the previous subsections. Furthermore, the respective condition associated with C_{33} reads

$$\frac{\partial \Psi}{\partial C_{33}} = 0 \quad \Leftrightarrow \quad \frac{1}{2} \mathbf{S} : (\mathbf{E}_3 \otimes \mathbf{E}_3) = 0 \quad (58)$$

As a consequence, the stresses resulting from energy relaxation fulfill indeed the plane stress condition. It bears emphasis that in case of vanishing shear strains $(\bullet)_{i3}$, Eq. (58) is equivalent to $\sigma_{33} = 0$ where $\boldsymbol{\sigma}$ denotes the Cauchy stresses.

Remark 7. The implementation of the three-dimensional model is almost identical to that fulfilling a priori plane stress conditions. More precisely, within the resulting 3D finite element formulation, a minimization with respect to C_{33} is performed first. Subsequently, the wrinkling criteria according to Subsection 3.2 are checked. In case of slacks, the solution follows directly from Subsection 3.2.1. On the other hand, if the formation of wrinkles is signalled, the state variables are computed from Eq. (57). The respective derivatives necessary for an optimization algorithm are given by Eq. (58) and in Subsection 3.3.1. The second derivatives can be derived similarly. However, for the sake of brevity, they are omitted here.

3.5 Modifications necessary for initial stresses

Membranes often show initial stresses, e.g. resulting from prestress. Clearly, these stresses can be modeled simply by applying the respective loading history. Alternatively, the Helmholtz energy of the constitutive model can be modified. In the following, \mathbf{S}_0 denotes the initial stresses (of second Piola-Kirchhoff type) and \mathbf{F}_0 is a (possibly incompatible) deformation gradient characterizing the previous loading history. Hence, with $\mathbf{F} = \text{GRAD}\varphi$, the effective deformation gradient reads

$$\mathbf{F}_{\text{eff}} := \mathbf{F} \cdot \mathbf{F}_0 \quad (59)$$

and the resulting free energy is given by

$$\Psi_{\text{eff}}(\mathbf{C}) := \Psi(\mathbf{C}_{\text{eff}}), \quad \mathbf{C}_{\text{eff}} := \mathbf{F}_{\text{eff}}^T \cdot \mathbf{F}_{\text{eff}} = \mathbf{F}_0^T \cdot \mathbf{C} \cdot \mathbf{F}_0 \quad (60)$$

The initial strains \mathbf{F}_0 can be computed from the constraint

$$\mathbf{S}_0 = 2 \mathbf{F}_0^{-1} \cdot \left. \frac{\partial \Psi_{\text{eff}}}{\partial \mathbf{C}_{\text{eff}}} \right|_{\mathbf{C}_{\text{eff}} = \mathbf{F}_0^T \cdot \mathbf{F}_0} \cdot \mathbf{F}_0^{-T} \quad (61)$$

Clearly, in case of wrinkling, the effective right Cauchy-Green tensor yields now

$$\mathbf{C}_{\text{eff}} = \mathbf{F}_0^T \cdot (\mathbf{C} + \mathbf{C}_w) \cdot \mathbf{F}_0 \quad (62)$$

and the wrinkling parameters can be obtained in the same manner as described before.

It bears emphasis that the variational h -adaption which will be presented in the next section can be applied to any minimization problem; in particular to that discussed here. As a result, the novel mesh adaption allows to take prestress consistently into account.

4 Variational h -adaptivity

The proposed numerical framework suitable for the analysis of wrinkles and slacks is directly governed by the underlying variational principle. In case of hyperelasticity, this principle is that of the minimum potential energy. The advantages resulting from such a variational structure are manifold. For instance, it opens up the possibility to apply standard optimization strategies to solve the considered problem as shown in the previous section. Moreover, minimization principles provide a natural basis to estimate the quality of the numerical solution and hence, they represent a natural basis for mesh adaption. Such variational mesh adaptations were advocated in [23] in case of an Arbitrary Lagrangian-Eulerian (ALE) formulations, while a variational h -adaption was presented in [24]. For an overview, the interested reader is referred to [32]. In this section, the h -adaptive finite element method discussed in [24] is slightly modified and combined with the energy driven wrinkling algorithm as proposed in Section 3. It should be noted that this section is not meant to be a comprehensive overview on adaptive finite elements methods. For instance, so-called goal-oriented methods are not covered at all. For further details on mesh adaption, the reader is referred to [33–35].

According to [24], the (modified) principle of minimum potential energy (23) provides an unambiguous comparison criterion for test functions: a test function $\varphi^{(1)}$ is *better* than another $\varphi^{(2)}$ if *and only if* $I(\varphi^{(1)}) < I(\varphi^{(2)})$. All other considerations are, in effect, spurious. This energy comparison criterion is the basis of variational mesh adaption. Based on this relatively simple observation, an error indicator of the type

$$\Delta \tilde{I} = \inf_{\varphi_h^{(1)}} I_h(\varphi_h^{(1)}) - \inf_{\varphi_h^{(2)}} I_h(\varphi_h^{(2)}) \quad (63)$$

can be introduced. Here, $\varphi_h^{(1)}$ is the deformation mapping spanned by the initial mesh and $\varphi_h^{(2)}$ is associated with a locally refined triangulation. Accordingly, $\Delta \tilde{I}$ checks the effect of local mesh refinement on the solution. In this work, attention is confined to simplicial meshes and edge bisection (cf [36–38]) as the device for achieving mesh refinement, Fig. 2. In what follows, σ_e denotes the transformation that refines an initial mesh $\mathcal{T}_h^{(1)}$ by bisection of edge e resulting in $\mathcal{T}_h^{(2)}$. Obviously, edge bisection generates a nested family of triangulations and hence, the space of admissible deformations is indeed enlarged ($\varphi_h^{(1)} \in V_h^{(1)} \subset V_h^{(2)} \ni \varphi_h^{(1)}$). As a result, $\Delta \tilde{I}_h(e) \geq 0$.

Unfortunately, the proposed error indicator is numerically very expensive. More precisely, a global optimization problem has to be solved for every edge. Therefore, the local energy released by mesh refinement is estimated by means of a lower bound obtained by relaxing a local patch of elements. With $\varphi_h^{(1)}$ being the solution of the initial mesh, i.e., $\varphi_h^{(1)} = \arg \inf I_h(\varphi_h^{(1)})$, the error indicator $\Delta I_h(e)$ as proposed in [24] reads

$$0 \leq \Delta I_h(e) := I_h(\varphi_h^{(1)}) - \inf_{\substack{\varphi_h^{(2)} \in V_2, \\ \varphi_h^{(2)}|_{\partial\Omega_1} = \bar{\varphi}, \\ \text{supp}(\varphi_h^{(2)} - \varphi_h^{(1)}) = \text{supp}(V_h^{(2)}/V_h^{(1)})}} I_h(\varphi_h^{(2)}) \leq \Delta \tilde{I}_h \quad (64)$$

It is computed for every edge e . Here, $\bar{\varphi}$ and $\text{supp}(f)$ are prescribed deformations acting at $\partial_1\Omega$ and the support of the function f , respectively. According to Eq. (64), the influence of local mesh refinement is estimated by relaxing the deformation field only in the refined region $\text{supp}(V_h^{(2)}/V_h^{(1)})$. Clearly this set is defined by all elements sharing the considered edge e . As a consequence, in the numerical implementation, the deformation mapping is fixed and identical to that of the initial mesh outside $\text{supp}(V_h^{(2)}/V_h^{(1)})$, while in the interior of $\text{supp}(V_h^{(2)}/V_h^{(1)})$ the

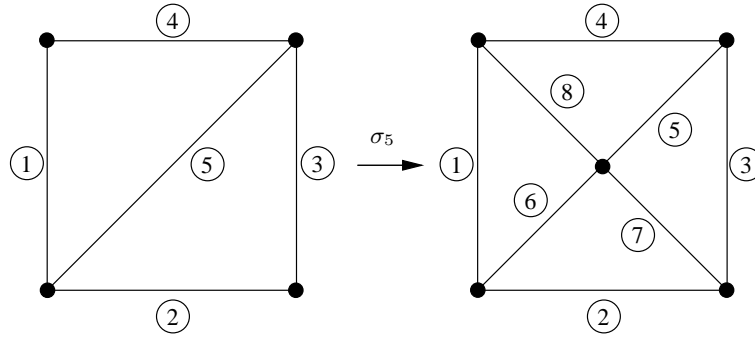


Figure 2: Mesh refinement in two dimensions by applying edge-bisection; σ_e denotes the transformation that refines an initial mesh by bisection of edge e

nodal displacements are computed by minimizing the respective energy. Further details on the presented variational indicator are omitted. They may be found in [24, 32].

The error measure (64) shows $O(n)$ complexity and therefore, can be computed efficiently. Having calculated ΔI_h for each edge within the triangulation, the edges are sorted accordingly and the limits

$$\mu_{\text{loc}}(\mathcal{T}_h) = \max_e \Delta I_h(e), \quad \rho_{\text{loc}}(\mathcal{T}_h) = \min_e \Delta I_h(e) \quad (65)$$

can be specified. Finally, the following mesh refinement strategy is employed:

i) For all edges in \mathcal{T}_h DO:

$$\text{IF } \Delta I_h(e) > \alpha_{\text{ref}} (\mu_{\text{loc}}(\mathcal{T}_h) - \rho_{\text{loc}}(\mathcal{T}_h)) + \rho_{\text{loc}}(\mathcal{T}_h), \text{ mark } e \text{ for refinement.}$$

ii) Apply refinement.

Here, $\alpha_{\text{ref}} \in (0, 1]$ is a numerical parameter defining the threshold of the edges to be cut.

Remark 8. Within the numerical examples presented in Section 5 only the energetically most favorable edge is cut at a time. Hence, $\alpha_{\text{ref}} = 1$.

Remark 9. The algorithm presented in this subsection is not stable. Consequently, degenerated elements can occur (the aspect ratios of the elements created by this method can converge to infinity). As a consequence, as shown in [24, 32], if only edges which have been marked by the presented error indicator are cut, the resulting meshes can be highly anisotropic. However, this anisotropy is related to the physics of the considered problem and therefore, the performance of those meshes is superior to that of their isotropic counterparts, cf. [24]. It should be noted that in some cases, e.g., if iterative solvers are used, the aspect ratio of the elements may need to be maintained. In such a case, edges can be bisected by means of Rivara's longest-edge propagation path (LEPP) bisection algorithm [36–39], which guarantees an upper bound on the element aspect ratio. The performance of this method is shown in Section 5 as well.

Remark 10. In the case of linearized elasticity theory, it can be shown that the proposed error indicator is equivalent to a mathematically rigorously derived error estimate based on local Dirichlet problems, cf. [40, 41]. The respective proof can be found in [32]. Hence, in this case, the advocated error indicator inherits the same properties as the estimate according to [40, 41]. However, it should be noted that this equivalence is not fulfilled in the more general case. For highly non-linear problems, it is usually not even known, if an analytical solution exists, and even if it exists, it is not clear, if it is unique.

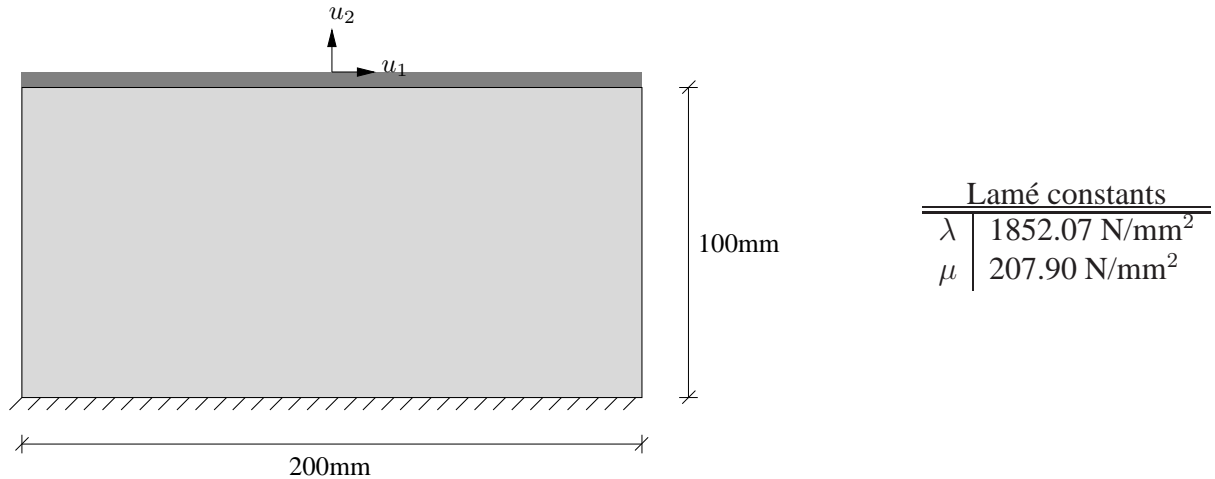


Figure 3: Shear test of a membrane: geometry (thickness of the membrane $t = 0.2$ mm) and material parameters (hyperelastic constitutive model according to Appendix A); boundary conditions: First, loading is applied by prescribing a vertical displacements of magnitude $u_2 = 1$ mm and $u_1 = 0$. Subsequently, u_1 is increased up to $u_1 = 10$ mm by holding fixed $u_2 = 1$ mm.

5 Numerical examples

The applicability and versatility of the variational wrinkling algorithm as well as the performance of the novel variational h -adaption are illustrated by means of two numerical examples. Particularly, the convergence rate of the proposed variational mesh adaption is highlighted. While a shear test is analyzed in Subsection 5.1, torsion of a circular membrane is computed in Subsection 5.2.

5.1 Shear test

The material parameters, the geometry and the boundary conditions of the first example are shown in Fig. 3. According to Fig. 3, tension is applied during the first loading stage, i.e., $u_2 = 1$ mm and $u_1 = 0$. Subsequently, u_1 is increased up to a final magnitude of $u_1 = 10$ mm by holding $u_2 = 1$ mm constant. The mechanical problem is identical in every way to that treated in [6] with the sole exception that a different constitutive model is used. Here, the hyperelastic potential described in Appendix A is adopted. However, it should be noted that the occurring strains are relatively small and hence, the considered material model predicts almost the same response as the isotropic version of the constitutive law in [6].

The response of the membrane is baselined by means of a relatively fine discretization (327.530 DoFs) consisting of 6-node quadratic triangle elements, see Fig. 4(a). Five different computations have been performed. Four of those are based on the minimization algorithm explained in the previous section. The resulting local and global optimization problems have been solved by applying a conjugate gradient approach of Fletcher-Reeves and Polak-Ribiere type [29], a limited memory BFGS method [30] and a damped Newton's scheme, cf. [31]. Additionally, a semi-analytical method has been used as well. In this case, the minimization problem characterizing the formation of wrinkles and slacks is solved analytically. The respective equations are summarized in Appendix A. As expected, the predicted mechanical response is independent of the applied solution scheme. The computed final deformed configuration, together with the distribution of the wrinkling strains, is shown in Fig. 4(a). Here, the larger eigenvalue of the wrinkling strain C_w is plotted. According to Fig. 4(a), wrinkles form at the

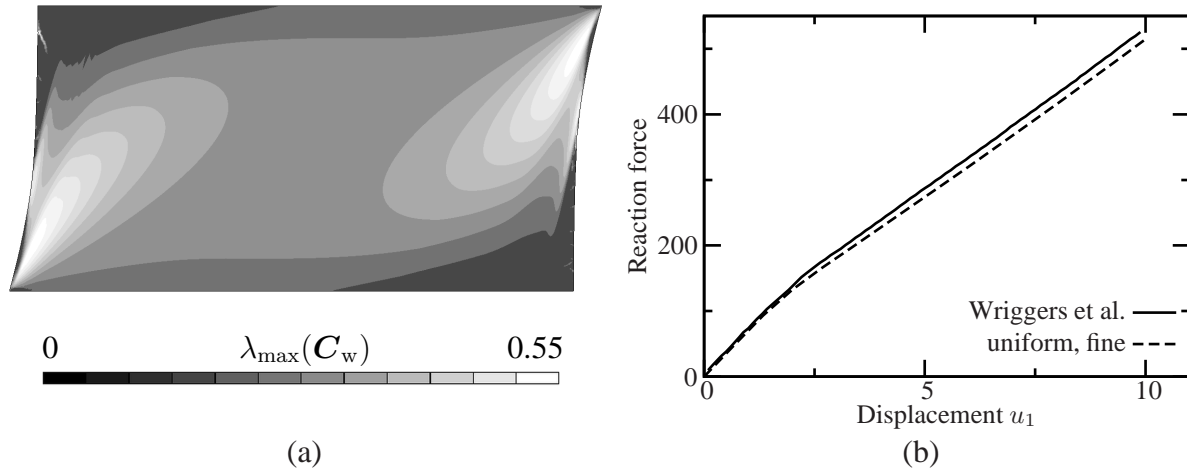


Figure 4: Shear test of a membrane: (a) final deformed configuration and distribution of the wrinkling strain $\lambda_{\max}(\mathbf{C}_w)$ computed by means of a uniformly fine discretization consisting of 6-node bi-quadratic triangle elements (327.530 DoFs); and (b) resulting load-displacement diagram (u_1 vs. conjugate force)

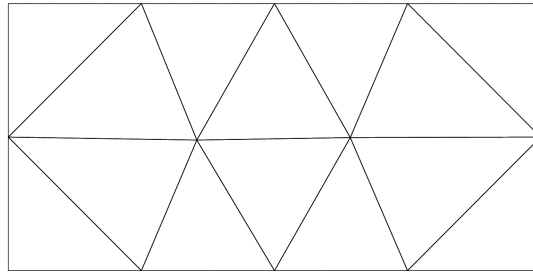


Figure 5: Shear test of a membrane: initial coarse discretization used for the adaptive finite element computations

lower left as well as at the upper right part of the membrane. Clearly, it is not known, if Fig. 4(a) corresponds to wrinkles or slacks in general. However, for the analyzed structure only a few slacks which are not shown explicitly develop at the upper left and the lower right part of the structure. Consequently, Fig. 4(a) is almost exclusively associated with wrinkles. It should be noted that the distributions of both the wrinkles as well as the (not shown) slacks agree with those reported in [6]. This can also be verified by the load-displacement diagram in Fig. 4(b). The proposed wrinkling algorithm, in conjunction with a relatively fine discretization, predicts an only marginally softer structural response than the numerical model presented in [6].

Next, the mechanical problem is re-analyzed by employing the h -adaptive scheme as discussed in Section 4. For that purpose, a computation based on the coarse discretization in Fig. 5 is performed first. Subsequently, the solution is improved by applying two different variational h -adaptions: an unconstrained variational h -adaptation calculation according to Section 4, in which only the energetically most favorable edge is bisected at each step; and a constrained variational h -adaptation calculation, in which an upper bound on the aspect ratio of the elements is maintained by means of Rivara's longest-edge propagation path (LEPP) bisection algorithm, cf. Remark 9.

Fig. 6 shows the adaptively computed meshes, the deformed configurations and the distribution of the wrinkling strain. By comparing the plots of the wrinkling strain in Fig. 6 to that

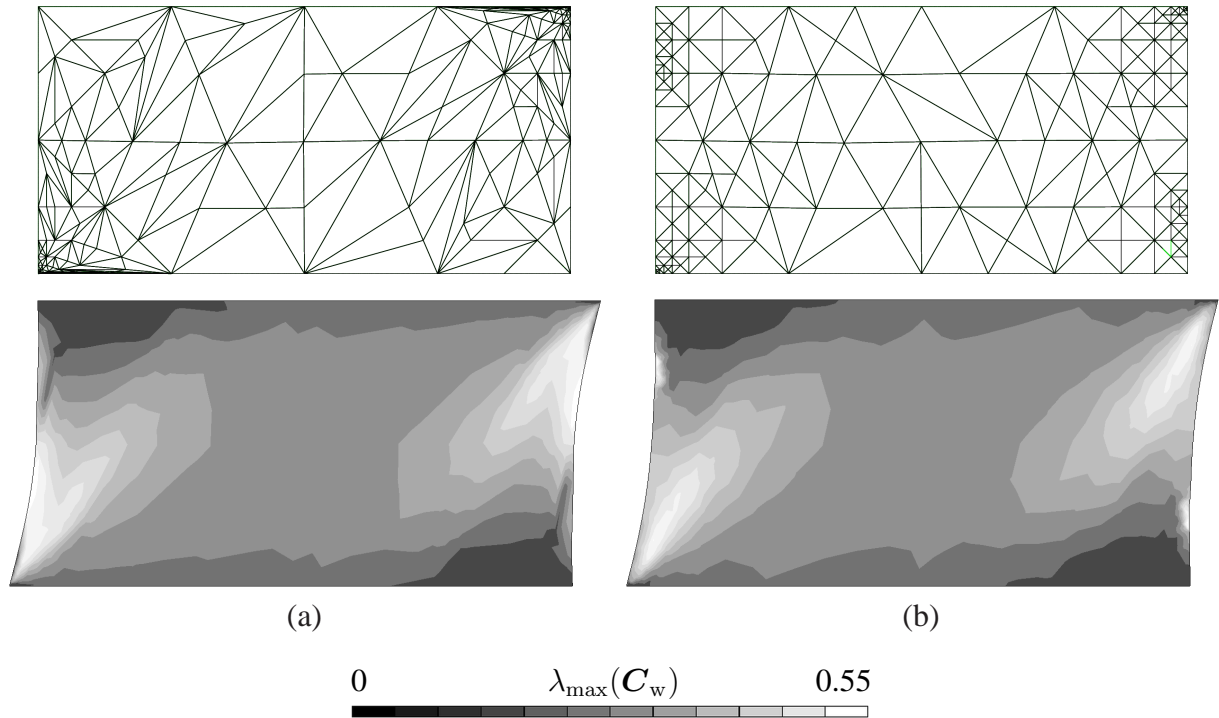


Figure 6: Shear test of a membrane: final meshes, deformed configurations, together with the distribution of the wrinkling strain $\lambda_{\max}(\mathbf{C}_w)$, after: (a) variational h -adaption; and (b) variational h -adaption combined with Rivara’s longest-edge propagation path (LEPP) bisection algorithm

corresponding to the fine discretization (Fig. 4(a)), the performance of the proposed variational mesh adaption becomes evident: Although the mesh computed by applying the unconstrained (constrained) h -adaption consists of only 582 (597) nodes (in contrast to 163765 nodes), it predicts an almost identical wrinkling pattern.

The quality of the numerical approximation associated with the variational mesh adaptations can be investigated best by analyzing the convergence in energy. The respective diagram is shown in Fig. 7. According to Fig. 7, the convergence rate of the adaptive scheme is remarkable. Although the final meshes resulting from the variational adaption are relatively coarse (582 and 597 nodes), the error in energy (with reference to the finest uniform discretization) is negligibly small (0.02%). Furthermore, as already noted in [24], constraining the aspect ratio of the elements has a detrimental effect on the rate of convergence. However, for the considered example, the decrease in performance is only marginal compared to the fully unconstrained algorithm.

5.2 Torsion of a circular membrane

The next example is concerned with a circular membrane subjected to torsion, Fig. 8. A similar problem has been investigated by several researchers, cf. e.g. [5, 7, 26]. Here, the geometry and the material parameters are chosen according to [42] with the sole exception that plastic effects are neglected. The membrane having a thickness of $t = 0.01\text{mm}$ is clamped at the outer as well as at the inner boundary and loading is applied by increasing the angle α at the inner boundary up to $\alpha_{\max} = 1.8^\circ = 0.03176\text{rad}$.

Following the previous subsection, three different computations have been performed. Start-

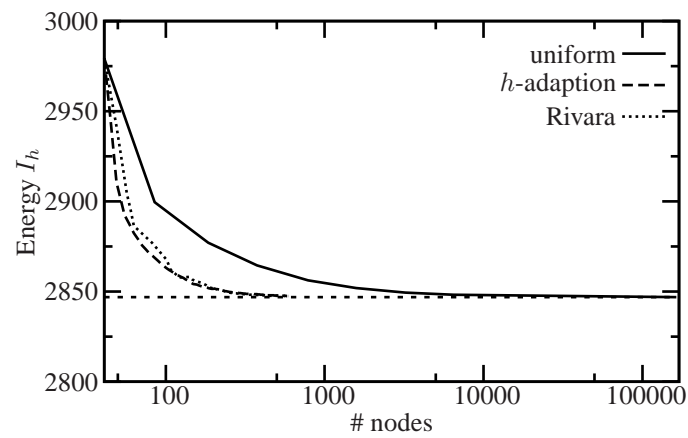
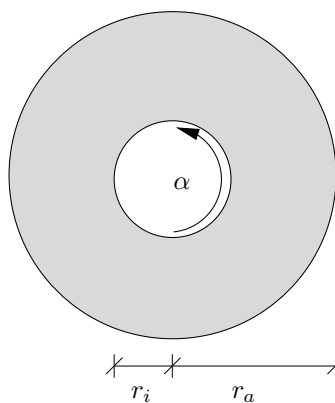


Figure 7: Shear test of a membrane: Convergence in energy resulting from: variational h -adaption; and variational h -adaption combined with Rivara's longest-edge propagation path (LEPP) bisection algorithm



Lamé constants	
λ	40384.615 N/mm ²
μ	26923.077 N/mm ²

Geometry	
r_a	125 mm
r_i	45 mm
t	0.01 mm

Figure 8: Torsion of a circular membrane: geometry, material parameters (hyperelastic constitutive model according to Appendix A) and boundary conditions. The membrane is clamped at both radii.

ing with the initially coarse discretization shown in Fig. 9 (top left), the mesh is refined subsequently by applying: the unconstrained h -adaption discussed in Section 4; and the variational h -adaptive scheme combined with Rivara's method for maintaining the aspect ration. It should be noted that the implemented edge-bisection method inserts new nodes in such a way that the boundary of the initial mesh is not modified. Since a bi-quadratic isoparametric formulation is applied here, the boundaries of the initial mesh, and as a result those of the refined discretizations, are no circles, but quadratic approximations. Consequently, the boundaries $\partial\Omega$ are not smooth ($\partial\Omega \notin \mathcal{C}^1$) resulting in artificial singularities. However, it bears emphasis that these effects have only a weak influence on the numerical solution (difference in energy is less than 0.5%). Furthermore, the insertion of new nodes at the boundaries can be easily modified such that the resulting curves converge to circles.

Fig. 9 summarizes the results computed from the different strategies. For the sake of comparison, uniform refinement is considered as well. At the top right in Fig. 9 the computed wrinkling distribution predicted by uniformly refining the coarse discretization at the top left in Fig. 9 is shown. The respective mesh which is not presented consists of 133640 nodes. According to this plot, the wrinkling strain and thus, the strain-energy, displays a rapid variation in the radial direction, while it varies slowly in the orthogonal direction.

In contrast to the uniformly refined triangulation, the discretizations corresponding to the adaptive methods contain only 5001 nodes (each). Although the number of DoFs is relatively small, the wrinkling pattern associated with the variational h -adaption agrees perfectly with that of the uniform mesh, cf. Fig. 9. Hence, the adaptive method increases the numerical efficiency significantly. It bears emphasis that the unconstrained h -adaption results in highly anisotropic and directional meshes that trace the fine structure of the energy-density field, see Fig. 9.

Following the previous subsection, the quality of the numerical schemes is investigated by analyzing the convergence in energy. The respective diagram is shown in Fig. 10. As evident from Fig. 10, all refinement strategies converge to the same limiting value highlighted by the horizontal dashed line. Furthermore, the adaptive methods show a remarkably higher convergence rate. Analogous to the previous subsection, the unconstrained variational h -adaption is superior to that of constrained variational h -adaption. In contrast to the shear test analyzed in Subsection 5.1, the wrinkling pattern associated with the example studied here is more localized and highly anisotropic, i.e., wrinkles only occur in a relatively small region in the vicinity of the inner boundary and the distribution of the wrinkling strains strongly varies in the radial direction compared to the orthogonal direction. Clearly, this effect can be better taken into account by the unconstrained h -adaption in which the elements are allowed to show different length scales in orthogonal directions (see Fig. 9). As a consequence, the superiority of unconstrained h -adaption is even more pronounced compared to the previous example.

6 Conclusion

A fully variational finite element formulation suitable for the analysis of membranes has been presented in this paper. In contrast to previous numerical models and inspired by the works by Pipkin [13, 15], the state variables, together with the deformation mapping, follow jointly from minimizing an energy functional. The proposed framework is very general and does not rely on any material symmetry of the hyperelastic material model. The elaborated method allows to employ arbitrary, fully three-dimensional hyperelastic constitutive models directly. More specifically, plane stress conditions characterizing a membrane stress state are naturally included within the variational formulation. Hence, a numerically expensive projection of the material model to plane stress space is not required.

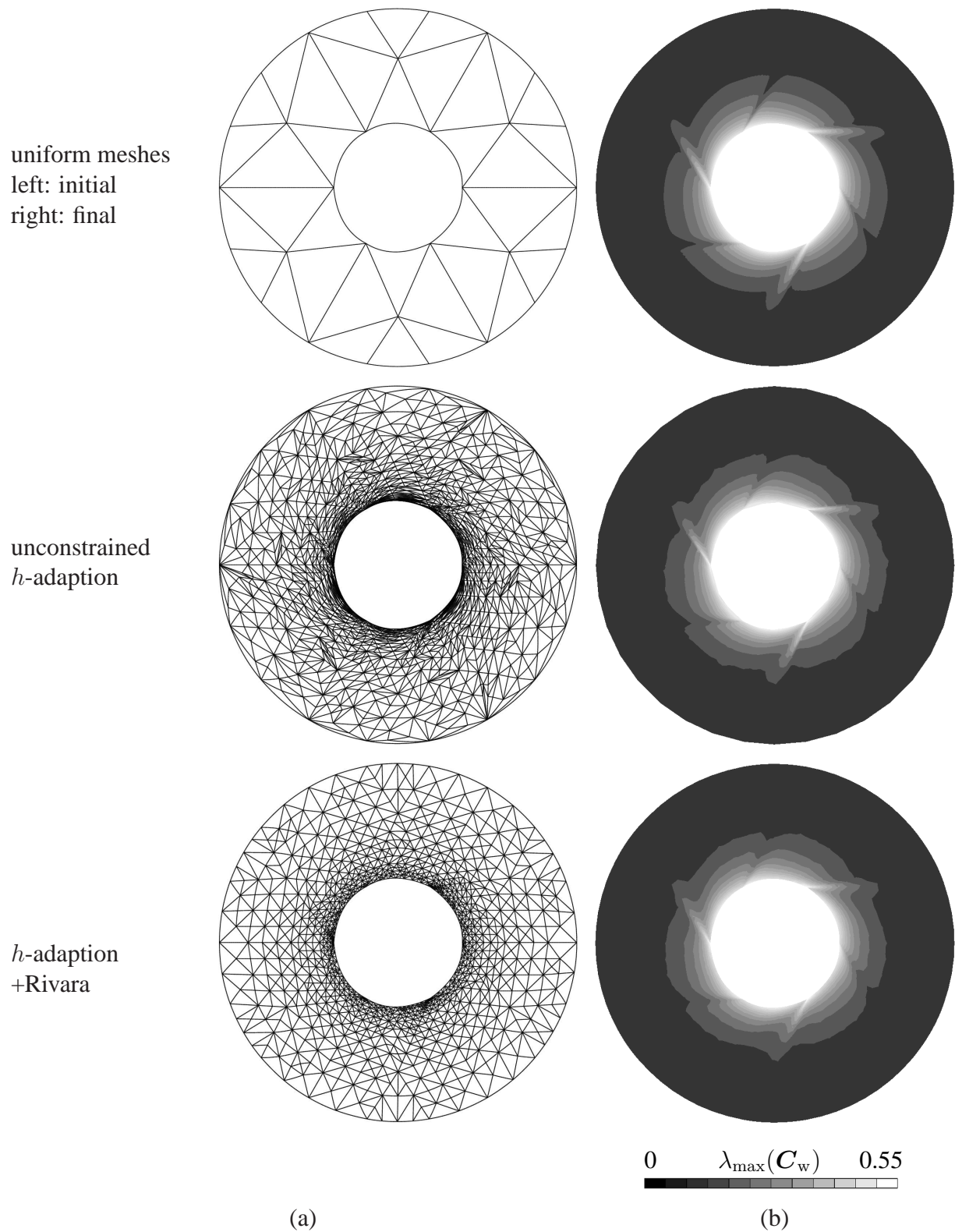


Figure 9: Torsion of a circular membrane: (a) initial mesh and discretizations predicted by the (un)constrained variational h -adaption; (b) distribution of the wrinkling strain $\lambda_{\max}(\mathbf{C}_w)$ resulting from: uniform refinement; and (un)constrained variational h -adaption

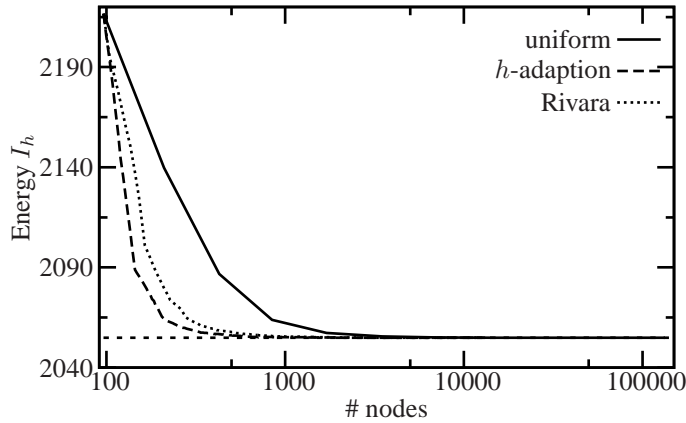


Figure 10: Torsion of a circular membrane: convergence in energy resulting from: variational h -adaption; and variational h -adaption combined with Rivara's longest-edge propagation path (LEPP) bisection algorithm

The numerical advantages associated with the advocated variational algorithmic method are manifold. For instance, it opens up the possibility of applying standard optimization methods to the numerical implementation. This is especially important for highly non-linear or singular problems such as wrinkling. Furthermore, the considered minimization problem is smooth with respect to the wrinkling parameters. Hence, the transition between the classical solution (no wrinkles or slacks) and the formation of wrinkles or slacks is smooth. This improves the stability and robustness of the resulting finite element formulation. An additional advantage associated with a minimization principle is that it provides a suitable basis for a posteriori error estimation and thus, for adaptive finite element formulations. As a prototype, a variational, physically and mathematically sound error indicator leading to an efficient h -adaption for wrinkling has been briefly discussed. The performance and robustness of the fully variational wrinkling approach has been demonstrated by selected finite element analyses. Particularly, the convergence rate of the proposed adaptive h -adaption is noteworthy.

A A stored energy functional for membranes

In this appendix, closed form solutions for an isotropic membrane constitutive model are given. In Section 5, the resulting equations are compared to the solutions obtained numerically by applying the proposed variational wrinkling algorithm. Starting with the three-dimensional polyconvex energy density (see [43])

$$\Psi = \lambda \frac{J^2 - 1}{4} - \left(\frac{\lambda}{2} + \mu \right) \log J + \frac{1}{2} \mu (\operatorname{tr} \mathbf{C} - 3) \quad (66)$$

with

$$J = \prod_{i=1}^3 \lambda_i, \quad \operatorname{tr} \mathbf{C} = \sum_{i=1}^3 \lambda_i^2 \quad (67)$$

plane stress requires

$$\partial_{\lambda_3} \Psi = 0 \quad \Rightarrow \quad \lambda_3 = \sqrt{\frac{\lambda + 2\mu}{\lambda \lambda_1^2 \lambda_2^2 + 2\mu}} \quad (68)$$

Here and henceforth, λ and μ are the Lamé constants. Inserting this relation into the free energy gives the functional

$$\Psi_{\text{plane}} = \frac{1}{2} \mu (\text{tr} \mathbf{C} - 2) - \frac{\lambda + 2\mu}{4} (2 \log J + \log[\lambda + 2\mu] - \log[\lambda J^2 + 2\mu]) \quad (69)$$

characterizing plane stress conditions. In Eq. (69), the right Cauchy-Green tensor is two-dimensional, i.e.,

$$J = \prod_{i=1}^2 \lambda_i, \quad \text{tr} \mathbf{C} = \sum_{i=1}^2 \lambda_i \quad (70)$$

In what follows the superscript $(\bullet)_{\text{plane}}$ is omitted.

A.1 Constitutive response for the standard solution without wrinkles or slacks

With Eq. (69), the two-dimensional stress state is computed as

$$\mathbf{S} = 2 \partial_{\mathbf{C}} \Psi = \mu \mathbf{1} - \frac{\mu (\lambda + 2\mu)}{J^2 \lambda + 2\mu} \mathbf{C}^{-1} \quad (71)$$

and the respective elastic tangent is given by

$$\mathbb{C} = 2 \partial_{\mathbf{C}} \mathbf{S} = \frac{2 J^2 \lambda \mu (\lambda + 2\mu)}{(J^2 \lambda + 2\mu)^2} \mathbf{C}^{-1} \otimes \mathbf{C}^{-1} + 2 \frac{\mu (\lambda + 2\mu)}{J^2 \lambda + 2\mu} \mathbf{C}^{-1} \underline{\otimes} \mathbf{C}^{-1} \quad (72)$$

Or equivalently,

$$\mathbf{P} = \mathbf{F} \cdot \mathbf{S} = \mu \mathbf{F} - \frac{\mu (\lambda + 2\mu)}{J^2 \lambda + 2\mu} \mathbf{F}^{-T} \quad (73)$$

$$\mathbb{A} = \partial_{\mathbf{F}} \mathbf{P} = \mu \mathbb{I} + \frac{\mu (\lambda + 2\mu)}{J^2 \lambda + 2\mu} \mathbf{F}^{-T} \underline{\otimes} \mathbf{F}^{-1} + \frac{2 J^2 \lambda \mu (\lambda + 2\mu)}{(J^2 \lambda + 2\mu)^2} \mathbf{F}^{-T} \otimes \mathbf{F}^{-T} \quad (74)$$

The non-classical tensor products used in this appendix are defined by $\{\mathbf{A} \overline{\otimes} \mathbf{B}\}_{ijkl} = A_{ik} B_{jl}$ and $\{\mathbf{A} \underline{\otimes} \mathbf{B}\}_{ijkl} = A_{il} B_{jk}$, respectively.

A.2 Constitutive response in case of slacks

Clearly, in case of slacks, the stresses vanish and so do the elastic tangent moduli of the material, i.e.,

$$\mathbf{S} = \mathbf{P} = \mathbf{0}, \quad \mathbb{C} = \mathbb{A} = \mathbf{0} \quad (75)$$

A.3 Constitutive response in case of wrinkles

According to Remark 6, for isotropic materials, the wrinkling directions \mathbf{N} and \mathbf{M} are the eigenvectors of the compatible right Cauchy-Green tensor \mathbf{C} . Hence, the eigenvalues $\tilde{\lambda}_i^2$ of the relaxed Cauchy-Green tensor \mathbf{C}_r are given by

$$\tilde{\lambda}_1^2 = \lambda_1^2, \quad \tilde{\lambda}_2^2 = \lambda_2^2 + a^2 \quad (76)$$

Inserting Eq. (76) into Eq. (69) and minimizing the energy over a^2 leads to

$$\tilde{\lambda}_2^2(\lambda_1) = -\frac{\mu}{\lambda \lambda_1^2} + \frac{\sqrt{\lambda^2 \lambda_1^2 + 2 \lambda \lambda_1^2 \mu + \mu^2}}{\lambda \lambda_1^2} \quad (77)$$

Finally, if Eq. (77) is inserted into Eq. (69), a relaxed energy density depending only on λ_1^2 can be derived, cf. [13]. Since this equation is relatively lengthy, it is omitted here. However, based on this energy density the stress response can be computed as

$$\mathbf{S} = S_M \mathbf{M} \otimes \mathbf{M} \quad (78)$$

where the principal stress is given by

$$S_M := \frac{\partial \Psi_r(\lambda_1)}{\partial \lambda_1} \frac{1}{\lambda_1} = \frac{\mu (\lambda \lambda_1^4 + \mu - \sqrt{\lambda^2 \lambda_1^2 + 2 \lambda \lambda_1^2 \mu + \mu^2})}{\lambda \lambda_1^4} \quad (79)$$

and \mathbf{M} is the eigenvector associated with the larger eigenvalue of \mathbf{C} . A further differentiation yields the elastic tangent moduli

$$\mathbb{C} = \underbrace{\frac{1}{\lambda_1} \frac{\partial}{\partial \lambda_1} \left(\frac{\partial \Psi_r(\lambda_1)}{\partial \lambda_1} \frac{1}{\lambda_1} \right)}_{=: D} \mathbf{M} \otimes \mathbf{M} \otimes \mathbf{M} \otimes \mathbf{M} + 2 S_M \partial_{\mathbf{C}}(\mathbf{M} \otimes \mathbf{M}) \quad (80)$$

with

$$D = \frac{\mu (3 \lambda^2 \lambda_1^2 + 6 \lambda \lambda_1^2 \mu + 4 \mu (\mu - \sqrt{\lambda^2 \lambda_1^2 + 2 \lambda \lambda_1^2 \mu + \mu^2}))}{\lambda \lambda_1^6 \sqrt{\lambda^2 \lambda_1^2 + 2 \lambda \lambda_1^2 \mu + \mu^2}} \quad (81)$$

The derivative of the eigenvectors $\mathbf{M} \otimes \mathbf{M}$ with respect to \mathbf{C} can be found elsewhere, cf. [44]. In this paper, the non-standard representation

$$\partial_{\mathbf{C}}(\mathbf{M} \otimes \mathbf{M}) = \frac{1}{\lambda_2^2 - \lambda_1^2} [\mathbb{I}^{\text{sym}} - \mathbf{N} \otimes \mathbf{N} \otimes \mathbf{N} \otimes \mathbf{N} - \mathbf{M} \otimes \mathbf{M} \otimes \mathbf{M} \otimes \mathbf{M}] \quad (82)$$

is used. Based on Eqs. (79) and (80) an equivalent constitutive response in terms of \mathbf{P} and \mathbb{A} can be derived. However, details are omitted.

References

- [1] H. Wagner. Ebene Blechwandträger mit sehr dünnen Stegblechen. *Z. Flugtechnik u. Motorluftschiffahrt*, 20, 1929.
- [2] E Reissner. On tension field theory. In *Fifth Int. Cong. on Appl. Mech.*, pages 88–92, 1938.
- [3] D.G. Roddeman, J. Drukker, C.W.J. Oomens, and J.D. Janssen. The wrinkling of thin membranes: Part I – theory. *Journal of Applied Mechanics*, 54:884–887, 1987.
- [4] D.G. Roddeman, J. Drukker, C.W.J. Oomens, and J.D. Janssen. The wrinkling of thin membranes: Part I – numerical analysis. *Journal of Applied Mechanics*, 54:888–892, 1987.
- [5] H. Schoop, L. Taenzer, and J. Hornig. Wrinkling of nonlinear membranes. *Computational Mechanics*, 29:68–74, 2002.
- [6] T. Raible, K. Tegeler, S. Löhnert, and P. Wriggers. Development of a wrinkling algorithm for orthotropic membrane materials. *Computer Methods in Applied Mechanics and Engineering*, 194:2550–2568, 2005.

- [7] M. Miyazaki. Wrinkle/slack model and finite element dynamics of membranes. *International Journal for Numerical Methods in Engineering*, 66:1179–1209, 2006.
- [8] D.J. Steigmann. Tension-Field theory. *Proceedings of the Royal Society of London. Series A, Mathematical and Physical Science*, 429:141–173, 1990.
- [9] F. Cirak, M. Ortiz, , and P. Schröder. Subdivision surfaces: A new paradigm for thin-shell finite-element analysis. *International Journal for Numerical Methods in Engineering*, 47:2039–2072, 2000.
- [10] F. Cirak and M. Ortiz. Fully c_1 -conforming subdivision elements for finite deformation thin-shell analysis. *International Journal for Numerical Methods in Engineering*, 51:813–833, 2001.
- [11] G. Gioia and M. Ortiz. Determination of thin-film debonding parameters from telephone-cord measurements. *Acta Metallurgica*, 46:169–175, 1997.
- [12] G. Gioia, A. DeSimone, M. Ortiz, and A.M. Cuitiño. Folding energetics in thin-films diaphragms. *Proceedings of the Royal Society of London. Series A, Mathematical and Physical Science*, 458:1223–1229, 2002.
- [13] A.C. Pipkin. The relaxed energy density for isotropic elastic membranes. *IMA Journal of Applied Mathematics*, 36:85–99, 1986.
- [14] A.C. Pipkin. Convexity conditions for strain-dependent energy functions for membranes. *Arch. Rational Mech. Anal.*, 121:361–376, 1993.
- [15] A.C. Pipkin. Relaxed energy densities for large deformations of membranes. *IMA Journal of Applied Mathematics*, 52:297–308, 1994.
- [16] B. Dacorogna. Quasiconvexity and relaxation of nonconvex problems in calculus of variations. *J. Func. Aanal.*, 46:102–18, 1982.
- [17] M. Epstein. On the wrinkling of anisotropic membranes. *Journal of Elasticity*, 55:99–109, 1999.
- [18] M. Ortiz and L. Stainier. The variational formulation of viscoplastic constitutive updates. *Computer Methods in Applied Mechanics and Engineering*, 171:419–444, 1999.
- [19] R. Radovitzky and M. Ortiz. Error estimation and adaptive meshing in strongly nonlinear dynamic problems. *Computer Methods in Applied Mechanics and Engineering*, 172:203–240, 1999.
- [20] M. Ortiz and E.A. Repetto. Nonconvex energy minimisation and dislocation in ductile single crystals. *J. Mech. Phys. Solids*, 47:397–462, 1999.
- [21] C. Miehe. Strain-driven homogenization of inelastic microstructures and composites based on an incremental variational formulation. *International Journal for Numerical Methods in Engineering*, 55:1285–1322, 2002.
- [22] C. Carstensen, K. Hackl, and A. Mielke. Non-convex potentials and microstructures in finite-strain plasticity. *Proc. R. Soc. Lond. A*, 458:299–317, 2002.

-
- [23] J. Mosler and M. Ortiz. On the numerical implementation of variational arbitrary Lagrangian-Eulerian (VALE) formulations. *International Journal for Numerical Methods in Engineering*, 67:1272–1289, 2006.
- [24] J. Mosler and M. Ortiz. h-adaption in finite deformation elasticity and plasticity. *International Journal for Numerical Methods in Engineering*, 2006. in press.
- [25] J. Mosler and M. Ortiz. A Variational Arbitrary Lagrangian-Eulerian (VALE) formulation for standard dissipative media at finite strains. *International Journal for Numerical Methods in Engineering*, 2007. submitted.
- [26] R. Rossi, M. Lazzari, R. Vitaliani, and E. Oñate. Simulation of light-weight membrane structures by wrinkling model. *International Journal for Numerical Methods in Engineering*, 62:2127–2153, 2005.
- [27] M. Epstein and M.A. Forcinito. Anisotropic membrane wrinkling: theory and analysis. *International Journal for Solids and Structures*, 38:5253–5272, 2001.
- [28] C.-C. Wang and C. Truesdell. *Introduction to rational elasticity*. Noordhoff International Publishing Leyden, 1973.
- [29] J.C. Gilbert and J. Nocedal. Global convergence properties of conjugate gradient methods. *SIAM Journal on Optimization*, 2:21–42, 1992.
- [30] D.C. Liu and J. Nocedal. On the limited memory method for large scale optimization. *Mathematical Programming B*, 45(3):503–528, 1989.
- [31] C. Geiger and C. Kanzow. *Numerische Verfahren zur Lösung unrestringierter Optimierungsaufgaben*. Springer, 1999.
- [32] J. Mosler. *On the numerical modeling of localized material failure at finite strains by means of variational mesh adaption and cohesive elements*. Habilitation, Ruhr University Bochum, Germany, 2007. www.tm.bi.rub.de/mosler.
- [33] R. Verfürth. *A review of a priori error estimation and adaptive mesh-refinement techniques*. Wiley-Teubner, 1996.
- [34] M. Ainsworth and J.T. Oden. *A Posterior Error Estimation in Finite Element Analysis*. Wiley, 2000.
- [35] A. Ern and J.-L. Guermond. *Theory and practice of finite elements*. Springer New York, 2004.
- [36] M.-C. Rivara. Local modification of meshes for adaptive and / or multigrid finite-element methods. *Journal of Computational and Applied Mathematics*, 36:79–89, 1991.
- [37] M.-C. Rivara and Ch. Levin. A 3-D refinement algorithm suitable for adaptive and multigrid techniques. *Communications in Applied Numerical Methods*, 8:281–290, 1992.
- [38] E. Bänsch. Local mesh refinement in 2 and 3 dimensions. *Impact of Computing in Science and Engineering*, 3:181–191, 1991.
- [39] M.-C. Rivara. New longest-edge algorithms for the refinement and/or improvement of unstructured triangulations. *International Journal for Numerical Methods in Engineering*, 40:3313–3324, 1997.

-
- [40] I. Babuška and W.C. Rheinboldt. Error estimates for adaptive finite element computations. *SIAM J. Numer. Anal.*, 15:736–754, 1978.
- [41] C. Bernadi, B. Métivet, and R. Verfürth. Analyse numérique d indicateurs d erreur. Technical Report 93025, Université Pierre et Marie Curie, Paris VI., 1993.
- [42] J. Hornig. *Analyse der Faltenbildung in Membranen aus unterschiedlichen Materialien*. PhD thesis, Technische Universität Berlin, 2004.
- [43] P. Ciarlet. *Mathematical elasticity. Volume I: Three-dimensional elasticity*. North-Holland Publishing Company, Amsterdam, 1988.
- [44] J.C. Simo. Numerical analysis of classical plasticity. In P.G. Ciarlet and J.J. Lions, editors, *Handbook for numerical analysis*, volume IV. Elsevier, Amsterdam, 1998.